Nonlinear dynamics of lipid-shelled ultrasound microbubble contrast agents

A. A. Doinikov[1] & P. A. Dayton[2]
[1]*Belarus State University, Belarus*
[2]*University of California, Davis, USA*

Abstract

Encapsulated gas microbubbles, known as contrast agents, are widely used in ultrasound medical applications. The present study is devoted to modelling of the spatio-temporal dynamics of lipid-shelled contrast agents. A theoretical model is proposed that describes the radial and translational motion of a lipid-shelled microbubble in an ultrasound field. The model approximates the behaviour of the lipid shell by the linear 3-constant Oldroyd constitutive equation, incorporates the translational motion of the bubble, and accounts for acoustic radiation losses due to the compressibility of the surrounding liquid. The values of the shell parameters appearing in the model are evaluated by fitting simulated radius-time curves to experimental ones. The results are then used for the simulation of the translational motion of contrast agent bubbles of various radii and the evaluation of the relationship between equilibrium radii of lipid-shelled agents and their resonance frequencies in the regime of nonlinear oscillation.
Keywords: contrast agents, encapsulated bubbles, lipid shell, ultrasound, radial oscillation, translational motion, resonance frequencies.

1 Introduction

Ultrasound contrast agents are micron-sized encapsulated gas bubbles which are produced by pharmaceutical companies for medical ultrasound applications [1]. They are normally injected into the bloodstream of the patient in order to increase blood-tissue contrast during an ultrasonic examination and thereby to improve the quality of ultrasonic images. Contrast agents are also used in targeted imaging and ultrasound-assisted localized drug delivery [2, 3]. Targeted agents are taken up by specific tissues or adhere to specific sites in the body.

WIT Transactions on Engineering Sciences, Vol 56, © 2007 WIT Press
www.witpress.com, ISSN 1743-3533 (on-line)
doi:10.2495/MPF070251

By enhancing the acoustic differences between normal and abnormal parts of organs, these tissue-specific agents improve the detectability of abnormalities, such as lesions, inflammatory processes and thrombi. In addition, targeted agents can carry drugs or genes to be delivered to a specific site or tissue, which provides great possibilities for a highly selective therapeutic action. The shell is necessary to prevent bubbles from fast dissolution in blood and coalescence. Proper theoretical description of the shell is of primary importance as it is the shell that determines many of the functional properties of contrast agents. The shell of currently available contrast agents is made of albumin, polymer, or lipid. The present study is devoted to modelling of the spatio-temporal dynamics and investigation of resonant properties of lipid-shelled contrast agents.

2 Theoretical model

Consider a spherical encapsulated gas bubble immersed in an unbounded liquid and undergoing radial oscillations in response to an imposed acoustic field. The gas in the bubble is separated from the encapsulating layer by interface 1 while the encapsulating layer is separated from the surrounding liquid by interface 2. The radial oscillation of the bubble will be described by the generalized Rayleigh–Plesset equation [4, 5]:

$$R_1\ddot{R}_1\left[1+\beta\frac{R_1}{R_2}\right]+\dot{R}_1^2\left[\frac{3}{2}+\beta\left(\frac{4R_2^3-R_1^3}{2R_2^3}\right)\frac{R_1}{R_2}\right]=\frac{1}{\rho_S}\left[P_{g0}\left(\frac{R_{10}}{R_1}\right)^{3\gamma}-\frac{2\sigma_1}{R_1}-\frac{2\sigma_2}{R_2}\right.$$

$$\left.-P_0-P_{ac}(x,t)+3\int_{R_1}^{R_2}\frac{\tau_{rr}^{(S)}(r,t)}{r}\,dr+3\int_{R_2}^{\infty}\frac{\tau_{rr}^{(L)}(r,t)}{r}\,dr\right], \qquad (1)$$

where $R_1(t)$ and $R_2(t)$ are the inner and the outer radii of the bubble shell, respectively, the overdot denotes the time derivative, $\beta=\left(\rho_L-\rho_S\right)/\rho_S$, ρ_S and ρ_L are the equilibrium densities of the shell and the surrounding liquid, respectively, P_{g0} is the equilibrium gas pressure inside the bubble, γ is the ratio of specific heats of the gas, R_{10} is the inner radius of the bubble shell at rest, σ_1 and σ_2 are the surface tension coefficients for the corresponding interfaces, P_0 is the hydrostatic pressure in the surrounding liquid, $P_{ac}(x,t)$ is the driving acoustic pressure at the location of the bubble, $x(t)$ is the spatial position of the centre of the bubble in an inertial frame, $\tau_{rr}^{(S)}$ and $\tau_{rr}^{(L)}$ are the stress deviators of the shell and the liquid, respectively, and r is the distance from the centre of the bubble. Note that eqn. (1) assumes that the surrounding liquid and the encapsulating layer are incompressible so that both the liquid velocity and the velocity inside the bubble shell are given by

$$v(r,t)=R_1^2(t)\dot{R}_1(t)/r^2, \qquad (2)$$

where $v(r,t)$ denotes the radial component of either the liquid velocity, if $r > R_2$, or the velocity inside the encapsulating layer, if $R_1 \le r \le R_2$. The assumption of incompressible shell also gives

$$R_2^3 - R_1^3 = R_{20}^3 - R_{10}^3, \tag{3}$$

where R_{20} is the outer radii of the bubble shell at rest. These equations are used in further calculations.

The rheological behaviour of the bubble shell will be approximated by the linear 3-constant Oldroyd model which can be expressed as [6]

$$\tau_{rr}^{(S)} + \lambda_{S1}\frac{\partial \tau_{rr}^{(S)}}{\partial t} = 2\eta_S\left(v_{rr} + \lambda_{S2}\frac{\partial v_{rr}}{\partial t}\right), \tag{4}$$

where $v_{rr} = \partial v/\partial r$ is the radial component of the rate-of-strain tensor, λ_{S1} is the relaxation time of the shell, η_S is the shear viscosity of the shell and λ_{S2} is the retardation time of the shell. Substitution of eqn. (2) into eqn. (4) yields

$$\tau_{rr}^{(S)} + \lambda_{S1}\frac{\partial \tau_{rr}^{(S)}}{\partial t} = -\frac{4\eta_S}{r^3}\left[R_1^2\dot{R}_1 + \lambda_{S2}\left(R_1^2\ddot{R}_1 + 2R_1\dot{R}_1^2\right)\right]. \tag{5}$$

Equation (5) suggests that $\tau_{rr}^{(S)}(r,t)$ can be written as

$$\tau_{rr}^{(S)}(r,t) = -4\eta_S D_S(t)/r^3. \tag{6}$$

Substituting eqn. (6) into eqn. (5) shows that the function $D_S(t)$ obeys the equation

$$D_S + \lambda_{S1}\dot{D}_S = R_1^2\dot{R}_1 + \lambda_{S2}\left(R_1^2\ddot{R}_1 + 2R_1\dot{R}_1^2\right). \tag{7}$$

The motion of the surrounding liquid will also be described by a linear 3-constant Oldroyd equation

$$\tau_{rr}^{(L)} + \lambda_{L1}\frac{\partial \tau_{rr}^{(L)}}{\partial t} = 2\eta_L\left(v_{rr} + \lambda_{L2}\frac{\partial v_{rr}}{\partial t}\right), \tag{8}$$

where η_L denotes the shear viscosity of the liquid, λ_{L1} is the relaxation time and λ_{L2} is the retardation time. Note that for $\lambda_{L1} = \lambda_{L2} = 0$, eqn. (8) reduces to the equation that describes a viscous Newtonian liquid so that equations of bubble motion derived below can be used in both cases, when the surrounding liquid is water, which is usually the case in laboratory experiments, and when the surrounding liquid is blood as in clinical applications, since the Oldroyd constitutive equation is an acceptable model for blood [7]. Substituting eqn. (2) into eqn. (8) and representing $\tau_{rr}^{(L)}(r,t)$ as

$$\tau_{rr}^{(L)}(r,t) = -4\eta_L D_L(t)/r^3, \tag{9}$$

one finds an equation for the function $D_L(t)$ to be

$$D_L + \lambda_{L1}\dot{D}_L = R_1^2\dot{R}_1 + \lambda_{L2}\left(R_1^2\ddot{R}_1 + 2R_1\dot{R}_1^2\right). \tag{10}$$

Equations (6) and (9) make possible the calculation of the integral terms in eqn. (1). Equation (1) can also be modified to take account of the translation motion of the bubble and acoustic radiation losses due to the compressibility of the surrounding liquid. The modification can be performed by directly adopting necessary corrections from a recent paper by Doinikov and Dayton [8]. The final equation takes the form

$$R_1\ddot{R}_1\left[1+\beta\frac{R_1}{R_2}\right]+\dot{R}_1^2\left[\frac{3}{2}+\beta\left(\frac{4R_2^3-R_1^3}{2R_2^3}\right)\frac{R_1}{R_2}\right]-\frac{1}{c}\frac{\rho_L}{\rho_S}H=\frac{\rho_L}{\rho_S}\frac{\dot{x}^2}{4}+\frac{1}{\rho_S}\left[P_{g0}\left(\frac{R_{10}}{R_1}\right)^{3\gamma}\right.$$

$$\left.-\frac{2\sigma_1}{R_1}-\frac{2\sigma_2}{R_2}-4\eta_L\frac{D_L(t)}{R_2^3}-4\eta_S\frac{D_S(t)\left(R_{20}^3-R_{10}^3\right)}{R_1^3R_2^3}-P_0-P_{ac}(x,t)\right], \tag{11}$$

where the function H is defined as

$$H=\left[1+\beta\frac{R_1}{R_2}\right]^{-1}\left\{R_1\frac{dG}{dt}+2R_1\dot{R}_1\ddot{R}_1\left[1+\beta\frac{R_1^4}{R_2^4}\right]+2\dot{R}_1^3\left[1+\beta\frac{R_1^4\left(2R_2^3-R_1^3\right)}{R_2^7}\right]\right\}, \tag{12}$$

c is the speed of sound in the liquid and G denotes the right-hand side of eqn. (11). The compressibility correction is given by the last term on the left-hand side of eqn. (11), while the first term on the right-hand side of eqn. (11) provides the coupling with the translational equation. This latter is given by

$$m_b\ddot{x}+\frac{2\pi}{3}\rho_L\frac{d}{dt}\left(R_2^3\dot{x}\right)=-\frac{4\pi}{3}R_2^3\frac{\partial}{\partial x}P_{ac}(x,t)+F_d, \tag{13}$$

where m_b is the mass of the bubble and F_d is the viscous drag force which is taken in the form of Oseen's law

$$F_d=-(\pi/4)\eta_L R_2\,\dot{x}\left(24+9\rho_L R_2\left|\dot{x}\right|/\eta_L\right). \tag{14}$$

Finally, for $D_S(0)=D_L(0)=0$, from eqn. (11) it follows that P_{g0} is given by

$$P_{g0}=P_0+2\sigma_1/R_{10}+2\sigma_2/R_{20}. \tag{15}$$

Thus, we have the set of four ordinary differential equations: radial equation (11), translational equation (13) and eqns. (7) and (10) for the functions $D_S(t)$ and $D_L(t)$. The set is supplemented with eqns. (3), (12), (14) and (15). The initial conditions can be specified as $R_1(0)=R_{10}$, $R_2(0)=R_{20}$,

$\dot{R}_1(0) = \dot{R}_2(0) = 0$, $x(0) = x_0$, $\dot{x}(0) = 0$ and $D_S(0) = D_L(0) = 0$. Solving these four equations simultaneously, we can obtain a radius-time curve and translational displacement for an encapsulated bubble of given size.

3 Validation of theoretical model

In order to estimate the values of the shell parameters appearing in the theoretical model, experimental data obtained for the contrast agent MP1950 by Dayton *et al* [9] were used. MP1950 is a phospholipid-shelled microbubble with a decafluorobutane core. The surrounding liquid used in [9] was water, which allows one to set $\lambda_{L1} = \lambda_{L2} = 0$. Bubbles were insonified with a single 20-cycle acoustic pulse with a pressure amplitude of 180 kPa and a centre frequency of 2.25 MHz. To evaluate the shell parameters, simulated radius-time curves were fitted by the least squares method to experimental curves for 18 bubbles with equilibrium radii from about 0.79 to 2.81 μm. The fit has revealed that the retardation time for lipid coatings is in fact zero. Therefore all simulations described below were performed at $\lambda_{S2} = 0$. Also, following considerations made by Marmottant *et al* [10], the surface tension at the gas-shell interface, σ_1, was set equal to zero. Thus, the fitting was in fact carried out by varying the three shell parameters: λ_{S1}, η_S and σ_2. The values of the other model parameters were $P_0 = 101.3$ kPa, $\rho_L = 1000$ kg/m^3, $\eta_L = 0.001$ Pa·s, $c = 1500$ m/s, $\gamma = 1.07$, $\rho_S = 1100$ kg/m^3 and $R_S = R_{20} - R_{10} = 2$ nm.

It has been found that the surface tension σ_2 varies in random manner, i.e., regardless of bubble size, between 0 and 0.038 N/m with a mean of 0.0133 N/m. Whereas the relaxation time λ_{S1} and the shell viscosity η_S demonstrate a clear increase with increasing equilibrium radii. The best-fit values of λ_{S1} and η_S for the 18 experimental radius-time curves are shown by circles in figs. 1(a) and 1(b), respectively, as a function of equilibrium bubble radius. In both figures, the solid line represents a polynomial regression for the best-fit values of the shell parameters. It is interesting to note that for both parameters, a relatively good agreement between the best-fit values and the regression curve is achieved assuming that λ_{S1} and η_S are linearly dependent on the equilibrium volume of the bubble, $V_{b0} = (4\pi/3)R_{20}^3$. The equations of the regression curves shown in figs. 1(a) and 1(b) are given by

$$\lambda_{S1} = 0.0125 + 0.0024R_{20}^3 = 0.0125 + 0.00057V_{b0}, \tag{16}$$

$$\eta_S = 1.25 + 0.14R_{20}^3 = 1.25 + 0.033V_{b0}, \tag{17}$$

where the units of R_{20}, λ_{S1} and η_S are microns, microseconds and Pa s, respectively.

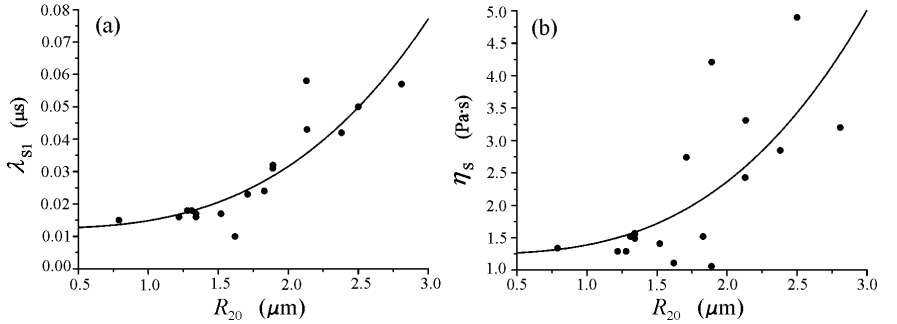

Figure 1: Best-fit values of (a) the relaxation time and (b) the shell viscosity as a function of equilibrium bubble radius. Each circle represents the best fit for one experimental radius-time curve. The solid lines show the polynomial regression of the fit values.

4 Numerical simulations

4.1 Translational motion

Equations (16) and (17), with $\sigma_2 = 0.0133$ N/m, were used to model translational displacement of lipid-shelled bubbles. The results obtained are displayed in fig. 2. The experimental translational displacement, adopted from [9], is shown by circles. The solid line indicates the simulated displacement calculated by the shell model proposed here, which treats the lipid shell as a viscoelastic fluid following the Oldroyd constitutive equation. For comparison, the dashed line shows the displacement that is predicted by the elastic shell model which treats the encapsulation as a viscoelastic solid following the Kelvin–Voigt constitutive equation, and the dotted line represents the results given by the viscous shell model which assumes that the encapsulating layer behaves as a viscous Newtonian fluid. The data for plotting these two curves were adopted from [11, 12]. One can see that the Oldroyd shell model provides better agreement with the experimental measurements than the two other models.

4.2 Resonance frequencies

The linear resonance frequency of a free bubble is known to be given by the Minnaert formula [13]. For the regime of nonlinear oscillations, there is no analytical formula and resonance frequencies can be evaluated solely by numerical calculations. In a classical paper by Lauterborn [14], resonance frequencies of free gas bubbles in the nonlinear regime are evaluated as follows. The quantity $\left(R_{\max} - R_0\right)/R_0$, called the normalized amplitude, is calculated numerically as a function of the frequency of the applied sound field, f, for different values of equilibrium bubble radius R_0. $R_{\max}$ denotes the maximum

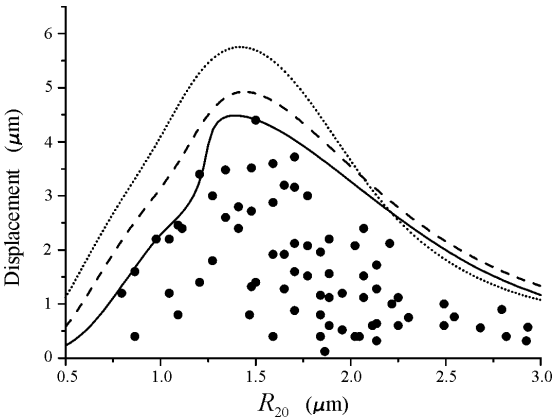

Figure 2: Experimental and simulated translational displacement as a function of equilibrium bubble radius. Circles indicate experimental results. The solid line corresponds to the Oldroyd shell model, the dashed line to the elastic (Kelvin–Voigt) shell model and the dotted line to the viscous shell model.

radius of the bubble during its steady-state oscillation. Normalized amplitude-frequency plots are called frequency response curves. Note also that the applied sound field is assumed to be a continuous sinusoidal wave. The frequency of the main resonance of a bubble with equilibrium radius R_0 is then determined as that corresponding to the main peak of the frequency response curve obtained for this bubble. This approach is, however, not quite adequate in the case of medical ultrasonic applications where insonation is in the form of pulses which can consist of only a few acoustic cycles. It is also not convenient if resonance frequencies are evaluated from experimentally measured radius-time curves, since, due to random fluctuations and measurement errors, the amplitude of the measured oscillation is not constant even at the steady state. In addition, when experimental data are processed, we normally deal with a fixed driving frequency and a set of radius-time curves measured at this frequency for bubbles of different size. In other words, in experiments, the equilibrium bubble radius is a variable quantity rather than the driving frequency. For such cases, a different approach is proposed to be used. The following quantity is calculated:

$$W(f, R_0) = \frac{1}{T}\int_0^T \left(\frac{R(t)}{R_0} - 1 \right)^2 dt \,, \tag{18}$$

where $R(t)$ is the radius-time curve for a bubble with equilibrium radius R_0 which occurs at the driving frequency f, and T is the duration of the bubble oscillation. The quantity $W(f, R_0)$ will be referred to as the oscillation power hereinafter. The oscillation power is plotted as a function of R_0 at a fixed

frequency f. The resonance radius for this frequency is then determined as that corresponding to the main peak of this plot. Clearly this method can be applied to both theoretical and experimental radius-time curves. We have applied it to evaluate resonance frequencies of lipid-shelled bubbles using eqns. (16) and (17) for the shell parameters. The bubbles were assumed to be surrounded by water and insonified with a 20-cycle, 2.25 MHz, 180 kPa acoustic pulse. The results obtained are displayed in fig. 3. The dependence between the equilibrium radius and the frequency of resonance response for lipid-shelled bubbles is shown by the solid line. For comparison, the dashed line represents the dependence obtained for free bubbles at the same acoustic parameters. Figure 3 reveals that, in contrast to albumin-shelled bubbles whose resonance frequencies are always higher than those of free bubbles, the resonance frequencies of lipid-shelled bubbles, depending on bubble size, can be both lower and higher than those of free bubbles of equivalent size. There are two regions in the behaviour of the resonance frequencies of lipid-shelled bubbles; namely, the resonance frequencies of larger lipid-shelled bubbles are lower than those of free bubbles of equivalent size, while the resonance frequencies of smaller lipid-shelled bubbles exceed those of free bubbles. It should be noted, however, that the sharpness of resonance response decreases with decreasing bubble size so that the resonance response of smaller bubbles is less pronounced, much more flattened, than that of larger bubbles. This effect is illustrated by fig. 4 which shows the oscillation power as a function of equilibrium radius for lipid-shelled bubbles at two values of the driving frequency, all other parameters being the same as in fig. 3. One can see that the higher the driving frequency, the more flattened is the resonance peak. For sufficiently high frequencies, the resonance response vanishes totally.

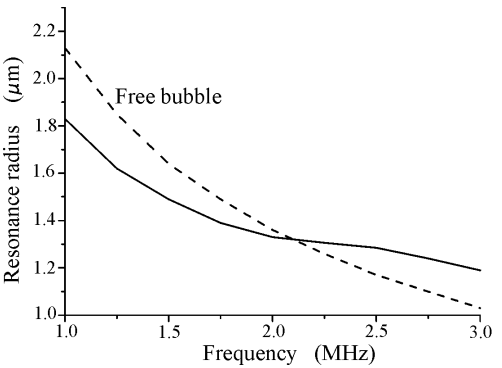

Figure 3: Dependence between the equilibrium radius and the frequency of resonance response for lipid-shelled bubbles in the regime of nonlinear oscillations. The excitation is a 20-cycle, 2.25 MHz, 180 kPa acoustic pulse. The dashed line represents the dependence for free bubbles at the same acoustic parameters.

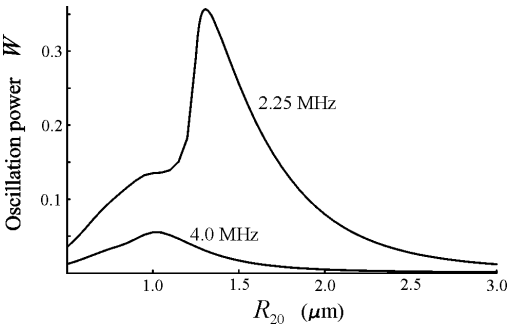

Figure 4: Oscillation power as a function of equilibrium radius for lipid-shelled bubbles at two values of the driving frequency.

This effect is explained by a strong damping impact of the shell viscosity on the oscillation of small encapsulated bubbles. A similar effect was pointed out earlier for polymeric- and albumin-shelled bubbles by Khismatullin [15] and Doinikov and Dayton [8].

5 Summary

A new theoretical model for a lipid-shelled contrast agent microbubble has been proposed. The model treats the lipid coating as a viscoelastic fluid following the linear Oldroyd constitutive equation and incorporates the translational motion of the bubble. The translational displacement predicted by the new model was compared to the experimentally measured displacement and the predictions of two existing models which treat the encapsulation as a viscoelastic solid or a simple viscous fluid. It has been shown that the new model provides better agreement with the experimental measurements than the two other models.

An approach has been proposed for evaluating resonance frequencies of lipid-shelled bubbles in the regime of nonlinear oscillation. The approach is based on calculating the time-averaged power of bubble oscillation as a function of equilibrium bubble radius at a given driving frequency. The resonance radius is then determined as that corresponding to the main peak of the oscillation power-radius function. The proposed method was applied to estimate resonance frequencies of lipid-shelled bubbles insonified with a 20-cycle, 2.25 MHz, 180 kPa pulse. It has been shown that the lipid shell can both increase and decrease the resonance frequencies of encapsulated bubbles with respect to those of free bubbles of equivalent size.

Acknowledgement

This work was supported by the International Science and Technology Center (ISTC) under Contract B-1213.

References

[1] Becher, H. & Burns, P.N., *Handbook of Contrast Echocardiography*, Springer Verlag: Frankfurt and New York, 2000.

[2] Bloch, S.H., Dayton, P.A. & Ferrara, K.W., Targeted imaging using ultrasound contrast agents. *IEEE Engineering in Medicine & Biology Magazine*, **23**, pp. 18–29, 2004.

[3] Klibanov, A.L., Microbubble contrast agents: Targeted ultrasound imaging and ultrasound-assisted drug-delivery applications. *Investigative Radiology*, **41(3)**, pp. 354–362, 2006.

[4] Roy, R.A., Church, C.C. & Calabrese, A., Cavitation produced by short pulses of ultrasound. *Frontiers of Nonlinear Acoustics*, eds. M.F. Hamilton & D.A. Blackstock, *Proc. of the 12th ISNA*, Elsevier: London, pp. 476–481, 1990.

[5] Church, C.C., The effect of an elastic solid surface layer on the radial pulsations of gas bubbles. *Journal of the Acoustical Society of America*, **97(3)**, pp. 1510–1521, 1995.

[6] Bird, R.B., Armstrong, R.C. & Hassager, O., *Dynamics of Polymeric Liquids*, Wiley: New York, 1987.

[7] Khismatullin, D.B. & Nadim, A., Radial oscillations of encapsulated microbubbles in viscoelastic liquids. *Physics of Fluids*, **14(10)**, pp. 3534–3557, 2002.

[8] Doinikov, A.A. & Dayton, P.A., Spatio-temporal dynamics of an encapsulated gas bubble in an ultrasound field. *Journal of the Acoustical Society of America*, **120(2)**, pp. 661–669, 2006.

[9] Dayton, P.A., Allen, J.S. & Ferrara, K.W., The magnitude of radiation force on ultrasound contrast agents. *Journal of the Acoustical Society of America*, **112(5)**, pp. 2183–2192, 2002.

[10] Marmottant, P., van der Meer, S., Emmer, M., Versluis, M., de Jong, N., Hilgenfeldt, S. & Lohse, D., A model for large amplitude oscillations of coated bubbles accounting for buckling and rupture. *Journal of the Acoustical Society of America*, **118(6)**, pp. 3499–3505, 2005.

[11] Doinikov, A.A. & Dayton, P.A., Modeling of the oscillation and translation dynamics of lipid-shelled ultrasound microbubble contrast agents: Theory. *Journal of the Acoustical Society of America*, submitted.

[12] Doinikov, A.A. & Dayton, P.A., Modeling of the oscillation and translation dynamics of lipid-shelled ultrasound microbubble contrast agents: Comparison to experiments. *Journal of the Acoustical Society of America*, submitted.

[13] Leighton, T.G., *The Acoustic Bubble*, Academic Press: San Diego, 1994.

[14] Lauterborn, W., Numerical investigation of nonlinear oscillations of gas bubbles in liquids. *Journal of the Acoustical Society of America*, **59(2)**, pp. 283–293, 1976.

[15] Khismatullin, D.B., Resonance frequency of microbubbles: Effect of viscosity. *Journal of the Acoustical Society of America*, **116(3)**, pp. 1463–1473, 2004.